Improved models for runway debris lofting simulations

S. N. Nguyen, E. S. Greenhalgh and L. Iannucci
Department of Aeronautics, Imperial College
London, UK

R. Olsson
Swerea SICOMP AB, Mölndal
Sweden

P. T. Curtis
Physical Sciences Department
Dstl Porton Down, Salisbury
Wiltshire, UK

ABSTRACT

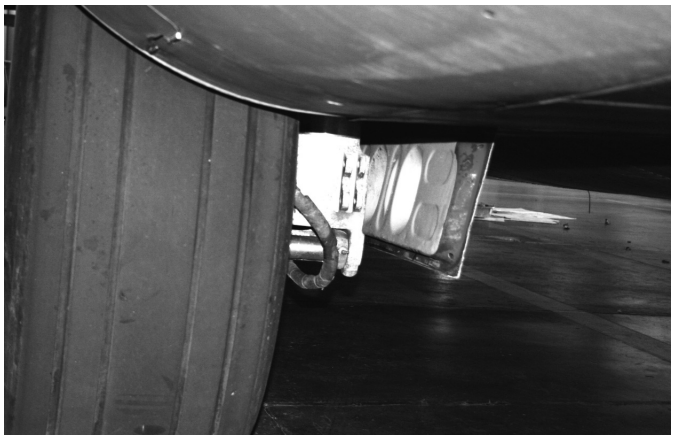
Numerical models used to simulate the lofting mechanisms of runway stones were developed to assess the threat to aircraft structures from runway debris impacts. An inflated aircraft tyre model, which was validated by comparison with experimental indentation tests, showed that over-rolling of stones under typical take-off conditions led to only modest vertical loft velocities of less than 5 m/s. Experiments using a drop weight impactor simulated a section of aircraft tyre descending upon stones. These tests demonstrated that lofting was achieved for impacts with low rubber thickness. However, for impacts with greater rubber thickness, lofting was suppressed. Using more realistic tyre geometries resulted in launches with backspin, but only horizontally along the ground in the direction of the tyre axis. The speed at which launches occurred was proportional to the rate of descent of the tyre section and would consequently determine the loft speeds due to potential asperity lofting.

NOMENCLATURE

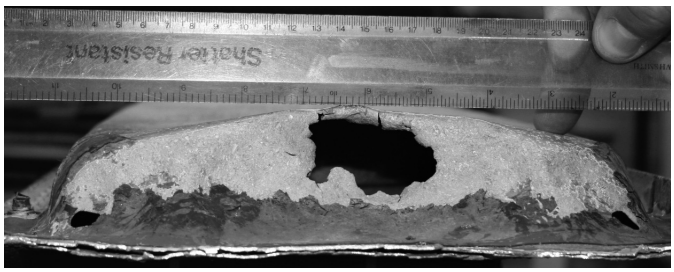
a	acceleration of aircraft (m/s^2)
B	coefficient in quadratic acceleration profile
c	ratio of aircraft velocity at end of nominal deceleration to velocity at touchdown
C	coefficient in quadratic acceleration profile
C_D	aerodynamic drag coefficient
C_L	aerodynamic lift coefficient
d	diameter of stone (m)
E_c	critical energy above which impact damage occurs (J)
F	aircraft factor describing the wheels and ground run performance parameters
F_D	aerodynamic drag force (N)
F_L	aerodynamic lift force (N)
g	acceleration due to gravity (ms^{-1})
h	height of impact point above ground (m)
H	horizontal distance between initial launch point of stone and impact point (m)
k_1	constant in quadratic acceleration profile
k_2	constant in quadratic acceleration profile
L	tyre rolling distance (m)
m	mass of stone (kg)
m_c	critical mass of stone (kg)
$\bar{m}$	constant in the Pareto function describing the stone mass distribution (kg)
M	constant in quadratic acceleration profile
n_d	number of stones of diameter d per unit area of runway
n_e	number of stones encountered
n_f	number of flights in the lifetime of an aircraft
n_m	number of main gear wheels that are able to loft stones
n_n	number of nose gear wheels that are capable of lofting stones
n_w	number of wheels on the aircraft
N	constant in quadratic acceleration profile
r	radius of stone (m)

Paper No. 3459. Manuscript received 1 June 2009, accepted 20 August 2009.

https://doi.org/10.1017/S000192400000333X Published online by Cambridge University Press



(a)



(b)

Figure 1. Photograph of a hole caused by stone impacts onto the leading edge of a C-130 Hercules inner bay door.

s_C	displacement of aircraft when it reaches the critical speed (m)
s_D	distance travelled by aircraft during acceleration from critical to take-off speed (m)
s_L	landing distance (m)
s_T	take-off distance (m)
S	spin factor
u	initial vertical velocity of lofted stone (ms^{-1})
v	velocity (ms^{-1})
v_c	critical speed below which no impact damage occurs (ms^{-1})
v_l	landing speed (ms^{-1})
v_t	take-off speed (ms^{-1})
v_e	aircraft speed at end of nominal deceleration phase (ms^{-1})
w	tyre footprint width (m)
α	constant in the Pareto function
β	constant in quadratic acceleration profile
λ	constant in quadratic acceleration profile
γ	constant in quadratic acceleration profile
μ	dynamic viscosity ($N\text{-}s/m^2$)
ρ	density (kg/m^3)
ω	angular velocity (rad/s)

1.0 INTRODUCTION

Runway debris lofted by aircraft tyres can cause considerable damage to aircraft structures (Fig. 1), yet there is limited understanding of the lofting mechanisms. The aim of this study was to develop accurate models to understand and predict the stone lofting processes. Such models will enable vehicle designers to determine the probability of a stone impact exceeding a critical velocity from a known distribution of debris over the runway surface[1]. The actual speed at which the stone is lofted might not be important; if launched at a high enough angle, the stone may reach a height such that the aircraft impinges on the stone. The research reported here entailed both finite element (FE) modelling and experimental validation using a modified drop weight impactor. Building upon previous work in this area[2,3], the significant simulation developments addressed in this paper include a study of the effect of the tyre geometry and modelling of an inflated tyre rolling over stones with real geometries i.e. based on objects actually collected from runways. The experimental investigation used an improved representation of a runway surface whilst determining the effect of different drop heights to relate stone impact conditions to the aircraft speed. Further experimental impacts studied the effect of the rubber thickness and used a section from a C-130 Hercules nose wheel tyre.

A number of potential stone loft mechanisms have been proposed and these have been grouped into two categories: tangential lofting or sideward lofting. A tyre partially rolling over a stone was expected to cause sideward lofting, whereas complete over-rolling would cause tangential lofting (Fig. 2(a)). Of the possible sideward lofting mechanisms proposed, three were considered in this study; hammer lofting, pinch launching and asperity lofting[4] (Fig. 2). Hammer lofting (Fig. 2(b)) occurs when a tyre deals a short, sharp downward blow to the upper surface of a stone. The resulting impulsive reaction from the ground causes lofting of the stone up and away from the tyre. Pinch launching (Fig. 2(c)) arises when a stone is squeezed between the tyre and ground until at some point the pressure causes the stone to squirt out and away from both surfaces, possibly with considerable backspin. Finally, asperity lofting (Fig. 2(d)) could occur if a stone travelling horizontally strikes an asperity protruding from the ground to then give the stone a vertical velocity component.

This paper firstly estimates the threat posed to aircraft, based on knowledge of the average areal density of debris distributed randomly over a runway. This threat was quantified in terms of the total number of stones that could potentially be thrown up by the wheels at speeds liable to cause damage upon impact to the aircraft. Based on the probability analysis in Section 2, and using data for the number of flights and wheels of various civil and military aircraft, the number of critical stone encounters can be estimated. As well as the distribution of stones on the runway, the impact damage threat is related to the probability of lofting, which the subsequent numerical simulations aimed to investigate. The development of improved inflated tyre and stone models and the results of lofting simulations are presented in Section 3. Drop weight experiments in Section 4 were used to confirm the influence of the improved tyre geometry in the simulations presented in Section 3. The discussion in Section 5

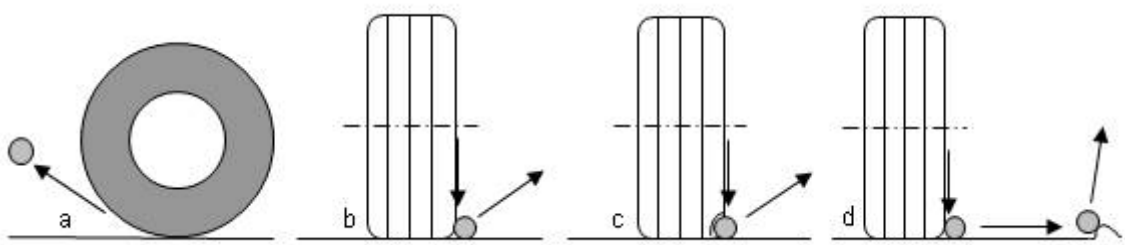


Figure 2. Potential lofting mechanisms: (a) tread flinging, (b) hammer (c) pinch (d) asperity lofting.

https://doi.org/10.1017/S000192400000333X Published online by Cambridge University Press

highlights a discrepancy between the observed impact damage presented in Section 1 and the results of the simulations in Section 3. This disagreement is explained by referring to the limitations of the modelling and experimental approaches used in Sections 3 and 4, leading to recommendations for further refinements followed by concluding remarks in Section 6.

2.0 PROBABILITY OF ENCOUNTERING A CRITICAL RUNWAY STONE

2.1 Tangential lofting

Firstly, consider a lofting mechanism described as simple tangential tread flinging (Fig. 2(a)), such that the normal impact velocity of the stone is equal to the tangential tyre speed[5]. Let n_d be the number of stones of diameter d per unit area of runway. The area swept out by one tyre with footprint width w and rolling distance L is wL. The number of stones of diameter d in this area is $n_d wL$. Let n_f be the total number of flights or take-offs (and landings) and n_w be the number of wheels on the aircraft. For wheels directly behind other wheels, such as the rear main wheels of a C-130 Hercules (Fig. 3), it was assumed that lofting occurs only from the front wheel, which was deemed to be 'active'. Therefore, a C-130 Hercules has four active wheels, since the nose wheels are side by side, whilst the main gear wheels are directly in line. The width of the tyre footprint was estimated as 84% of the full tyre width[6]. Assuming that the footprint width for all the wheels are equal and the landing distance is the same as the take-off distance, the number of stones encountered in the aircraft lifetime is

$$n_e = 2n_f n_w n_d wL \quad \ldots (1)$$

For the tread flinging mechanism, only stones in a certain zone within the tyre footprint need to be considered. Based on the severity of damage being primarily determined by the impact speed of the stone, the aircraft, and hence the stone, must travel above a critical speed v_c for damage to be inflicted. The critical speed for a composite structure for example may be specified as the delamination threshold velocity, which depends on the bending stiffness and mode II interlaminar toughness[7,8]. Since the mass of the stone has been shown to have little effect on the delamination threshold velocity[7,8] one might conclude that it is just as important to consider encounters with smaller stones. A larger mass implies a larger size and potentially a greater probability of loft[2,9] but the inherent probability of encountering larger stones is significantly smaller. For constant aircraft acceleration, a, the displacement s as a function of the aircraft speed v is given by $s = v^2 / (2a)$.

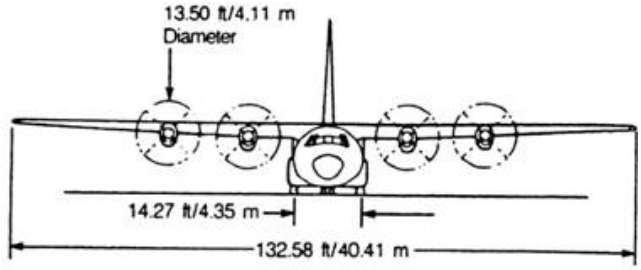
If aircraft speeds between the cut-off speed v_c and the take-off speed v_t can result in damage, these correspond to displacements along the runway s_C and s_T, between which there are critical stones. A critical runway length s_D can be defined as

$$s_D = s_T - s_C = \frac{v_t^2 - v_c^2}{2a} = \left[1 - \left(\frac{v_c}{v_t}\right)^2\right] s_T \quad \ldots (2)$$

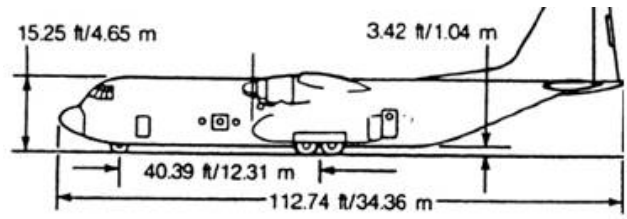
The same equation applies to calculate the proportion of the landing distance s_L within which stones can be lofted above the critical speed v_c when landing at speed v_l. Therefore, for a single flight, the total length of runway containing potentially damaging stones is given by;

$$s_D = \left[1 - \left(\frac{v_c}{v_t}\right)^2\right] s_T + \left[1 - \left(\frac{v_c}{v_l}\right)^2\right] s_L \quad \ldots (3)$$

The hazardous runway length s_D may be substituted in place of $2L$ in Equation 1 to give



(a)



(b)

Figure 3. C-130 Hercules aircraft (a) front view (b) left side view[10].

$$n_e = n_f n_w n_d w \left\{ \left[1 - \left(\frac{v_c}{v_l}\right)^2\right] s_T + \left[1 - \left(\frac{v_c}{v_l}\right)^2\right] s_L \right\} \quad \ldots (4)$$

If the nose and main tyres have different footprint widths, the required expression is

$$n_e = n_d F \text{ where } F = \left(n_n w_n + n_m w_m\right) \left\{ \left[1 - \left(\frac{v_c}{v_t}\right)^2\right] s_T + \left[1 - \left(\frac{v_c}{v_l}\right)^2\right] s_L \right\} \quad \ldots (5)$$

and n_n and n_m are the number of active nose and main wheels respectively, w_n and w_m are the corresponding footprint widths so that F is an aircraft specific factor.

2.1.1 Number of impacts

In a study of the distributions of stones collected from UK runways, the frequencies of stones per unit area with d > 5mm were $n_{d>5}$ = $11{\cdot}66 \times 10^{-4}\text{m}^{-2}$ and $n_{d>10}$ = $1{\cdot}84 \times 10^{-4}\text{m}^{-2}$ for stones with d > 10 mm[1]. Using characteristic operating data for a Hercules C-130 with four active wheels[10,11], nose and main footprint widths of 0·20m and 0·30m, take-off and landing speeds of 59ms^{-1} and 52ms^{-1}, take-off and landing distances of 457m and conducting 10,000 flights per aircraft lifetime[1], the expected number of potentially dangerous encounters with stones of d > 5mm above a cut-off speed of 30ms^{-1} was approximately 7,500. This value would need to be multiplied by the probability of loft P_L and the probability of impact given loft P_I to determine the total number of impacts n_I in a lifetime,

$$n_I = n_f n_d \left(n_n w_n + n_m w_m\right) \left\{ \left[1 - \left(\frac{v_c}{v_t}\right)^2\right] s_T + \left[1 - \left(\frac{v_l}{v_l}\right)^2\right] s_L \right\} P_L P_I \quad \ldots (6)$$

A first approximation would be to treat P_L and P_I as though they were independent of the stone properties. Findings from modelling of the lofting mechanisms can enable determination of the dependence of P_L and P_I on the most important parameters. Previous modelling studies[2] have suggested that the most salient variables to consider are, in order of decreasing importance: stone-tyre overlap, tyre edge radius, coefficients of static and dynamic friction, stone size, tyre stiffness, tyre speed, stone density and stone eccentricity.

https://doi.org/10.1017/S000192400000333X Published online by Cambridge University Press

For many military aircraft, operations on temporary or unpaved runways may be the main contributor to damage. Therefore, simply using data relating to the frequency of stones on UK RAF bases alone would not lead to a conservative estimate of the likely impact threat. Moreover, for any given take-off, the distribution of stones would not be best represented by all the stones collected in the runway sweepings over a period of time. Instead, assuming that between individual sweepings, the build up of stones and debris increased linearly, the average amount of debris encountered by an aircraft would be half the amount collected in sweepings over a given period. A similar characterisation of objects from civil airport runways would be needed to provide more accurate estimates of the likely encounters for civil aircraft.

2.1.2 Mass distribution

The distribution of the stone masses has been modelled by a two-parameter Pareto function[1].

$$f(m) = \frac{\alpha \bar{m}^{\alpha}}{m^{\alpha+1}} \quad \ldots (7)$$

The cumulative distribution function was found by integrating this probability density function to give

$$F(m) = 1 - \left(\frac{\bar{m}}{m}\right)^{\alpha} \quad \ldots (8)$$

The probability of a stone being over a certain mass m_c is therefore

$$P(m > m_c) = 1 - F(m_c) = \left(\frac{\bar{m}}{m_c}\right)^{\alpha} \quad \ldots (9)$$

where α and $\bar{m}$ are constants that describe the stone mass distribution. For a metal structure, such as the C-130 main wheel bay door, the impact energy was a suitable predictor of the severity of the damage. The probability of this energy E exceeding a critical energy E_c is given by

$$P(E > E_c) = \left(\frac{\bar{m}v^2}{2E_c}\right)^{\alpha} \quad \ldots (10)$$

2.1.3 Linear velocity profile for take-off

Assuming constant acceleration during take-off, the probability density function for the velocity of the stone in terms of the take-off speed v_t is given by

$$f(v) = \frac{1}{v_t} \quad \ldots (11)$$

The probability of the stone impacting at a speed v is given by

$$P(v) = f(v)\,\mathrm{d}v \quad \ldots (12)$$

Hence

$$P(E > E_c) = \sum_{v=0}^{v=v_t} P(v)P(E > E_c) \quad \ldots (13)$$

$$= \int_0^{v_t} f(v)\,P(E > E_c)\,\mathrm{d}v \quad \ldots (14)$$

$$= \frac{1}{v_t}\left(\frac{\bar{m}}{2E_c}\right)^{\alpha} \int_0^{v_t} v^{2\alpha}\,\mathrm{d}v \quad \ldots (15)$$

$$= \frac{1}{v_t}\left(\frac{\bar{m}}{2E_c}\right)^{\alpha} \left[\frac{v^{2\alpha+1}}{2\alpha+1}\right]_0^{v_t} \quad \ldots (16)$$

$$= \frac{v_t^{2\alpha+1}}{v_t(2\alpha+1)}\left(\frac{\bar{m}}{2E_c}\right)^{\alpha} \quad \ldots (17)$$

$$= \frac{1}{2\alpha+1}\left(\frac{\bar{m}v_t^2}{2E_c}\right)^{\alpha} \quad \ldots (18)$$

$$= \frac{(E_r/E_c)^{\alpha}}{2\alpha+1} \quad \ldots (19)$$

where the representative energy, $E_r = \frac{1}{2}\bar{m}\,v_t^2$, is related to the maximum energy that a representative stone can achieve. Using data for the normalised frequency distribution the masses of stones collected from UK RAF runways[1], the Pareto parameters determined from a least squares fit were $\alpha = 1{\cdot}645$ and $\bar{m} = 6 \times 10^{-4}$kg. The correlation coefficient was $R^2 = 0{\cdot}9999$. For $E_c = 50$ J and $v_t = 70\text{ms}^{-1}$, $P(E > E_c) = 0{\cdot}07\%$. Therefore, for 10,000 flights in a lifetime, and initially assuming that one impact occurs during every take-off and landing, the expected number of stones that impact with an energy of over 50J would be 14. Hence, for each take-off or landing, provided that the combined probability of a stone being encountered and lofted to cause an impact is less than 7%, the once-in-a-lifetime design threshold energy of 50J is adequate.

2.1.4 Quadratic acceleration profile for take-off

In reality, an improved fit to the velocity profile during take-off can be made using the assumption that the acceleration takes a quadratic relation with respect to the velocity[12],

$$a = Av^2 + Bv + C = A(v - M)(v - N) \quad \ldots (20)$$

where $M = \dfrac{-B - \sqrt{B^2 - 4AC}}{2A}$, $N = \dfrac{-B + \sqrt{B^2 - 4AC}}{2A}$

and A, B and C are constants found from a least squares fit to take-off performance data.

It can then be shown that the velocity may be expressed as a function of time using the following expression

$$v = \frac{M\left(1 - e^{k_1 t}\right)}{1 + k_2 e^{k_1 t}} \quad \ldots (21)$$

where $k_1 = A[M - N]$ and $k_2 = M/|N|$.

Rearranging to give time t in terms of velocity v,

$$t = \frac{1}{k_1}\ln\frac{M - v}{k_2 v + M} = \lambda \ln\frac{\beta - v}{k_2 v + \beta} \quad \ldots (22)$$

This effectively gives the cumulative distribution function of the velocity, which when differentiated gives the probability density function

$$f(v) = F'(v) = \frac{\mathrm{d}t}{\mathrm{d}v} = -\lambda\frac{k_2 v + \beta}{\beta - v}\frac{\beta(1 + k_2)}{(k_2 v + \beta)^2} \quad \ldots (23)$$

$$P(E > E_c) = \int_0^{v_t} f(v)\,P(E > E_c)\,\mathrm{d}v \quad \ldots (24)$$

$$= \int_0^{v_t} \frac{\gamma}{(v - \beta)(k_2 v + \beta)}\left(\frac{\bar{m}v^2}{2E_c}\right)^{\alpha} \mathrm{d}v \quad \ldots (25)$$

$$= \gamma\left(\frac{\bar{m}}{2E_c}\right)^{\alpha} \int_0^{v_t} \frac{v^{2\alpha}}{(v - \beta)(k_2 v + \beta)}\,\mathrm{d}v \quad \ldots (26)$$

where λ and β are constants of the normalised probability density function and $\gamma = \lambda\beta(k_2 + 1)$. This expression has no simple closed-form

https://doi.org/10.1017/S000192400000333X Published online by Cambridge University Press

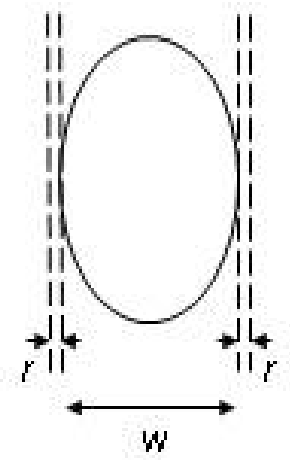


Figure 4. Plan view of area adjacent to tyre footprint within which a stone's centre of mass must lie to be lofted laterally.

solution but may be integrated numerically using Simpson's rule as in Ref. 1. The expression in Equation 26 can be closely pproximated to a second-order polynomial function of time t. An alternative approximation which allows for a closed form solution for the probability of exceeding a critical energy level is to use the following expression where time t is a polynomial function of the velocity v,

$$t = F(v) = \frac{1}{2}Av^2 + Bv + C \quad \ldots (27)$$

$$\frac{\mathrm{d}t}{\mathrm{d}v} = f(v) = Av + B \quad \ldots (28)$$

$$P(E > E_c) = \int_0^{v_t} f(v)\,P(E > E_c)\,\mathrm{d}v \quad \ldots (29)$$

$$= \left(\frac{\bar{m}}{2E_c}\right)^{\alpha} \int_0^{v_t} Av^{2\alpha+1} + Bv^{2\alpha}\,\mathrm{d}v \quad \ldots (30)$$

$$= \left(\frac{\bar{m}v_t^2}{2E_c}\right)^{\alpha} \left[\frac{Av_t}{2(\alpha+1)} + \frac{B}{2\alpha+1}\right] \quad \ldots (31)$$

$$= \left(\frac{E_r}{E_c}\right)^{\alpha} \left[\frac{Av_t}{2(\alpha+1)} + \frac{B}{2\alpha+1}\right] \quad \ldots (32)$$

where A has units of $(\mathrm{ms}^{-1})^{-2}$ and B has units of $(\mathrm{ms}^{-1})^{-1}$.

2.1.5 Landing velocity profile

The landing velocity profile takes a more complex form as there are four main phases after touchdown: initial braking, nominal deceleration, coasting and final deceleration to exit[13,14]. As a result, the assumption of constant deceleration leads to an over-conservative estimate of the probability of an impact exceeding a critical energy level. A suggested refinement would be to approximate the landing velocity profile using a bilinear function that models only two distinct deceleration phases: a nominal deceleration phase from the touchdown velocity v_t to a speed v_e at the end of this phase, followed by a reduced deceleration phase. The constant acceleration probability analysis would then be performed over these two separate velocity ranges, with the resulting probabilities summed to give the overall probability of exceeding a critical energy level.

$$P(E > E_c) = \frac{1}{2\alpha+1}\left(\frac{\bar{m}(v_t - v_e)^2}{2E_c}\right)^{\alpha} + \frac{1}{2\alpha+1}\left(\frac{\bar{m}v_e^2}{2E_c}\right)^{\alpha} \quad \ldots (33)$$

$$= \frac{1}{2\alpha+1}\left(\frac{\bar{m}}{2E_c}\right)^{\alpha}\left[(v_t - v_e)^{2\alpha} + v_e^{2\alpha}\right] \quad \ldots (34)$$

$$= \frac{(E_r/E_c)^{\alpha}}{2\alpha+1}\left[(1-c)^{2\alpha} + c^{2\alpha}\right] \quad \ldots (35)$$

where $c = v_e/v_t$. Depending on the landing velocity profile of a particular aircraft, it may be even more appropriate to use a linear nominal deceleration followed by a quadratic reduced deceleration phase. The corresponding probability can be derived using a combination of Equations (19) and (35) but is not included in the current paper.

The overall probability of a stone exceeding a critical energy level is the arithmetic mean of the individual expressions for take-off and landing given in Equations (35) and (38);

$$P(E > E_c) = \frac{1}{2}\left(\frac{E_r}{E_c}\right)^{\alpha}\left[\frac{Av_t}{2(\alpha+1)} + \frac{B}{2\alpha+1} + \frac{(1-c)^{2\alpha} + c^{2\alpha}}{2\alpha+1}\right] \quad \ldots (36)$$

2.2 Sideward lofting

Now consider lofting of a stone lying within a narrow zone at the sides of the tyre footprint (Fig. 4). A conservative analysis would assume that any overlap up to half the stone diameter may result in lofting. An overlap of more than half the stone was considered to be in the realm of tangential lofting as described in Section A. In this instance, the critical runway area within which stones must lie to be lofted is now reduced to dL and the corresponding number of impacts is

$$n_I = n_f n_d n_w d\left\{\left[1 - \left(\frac{v_c}{v_t}\right)^2\right]s_T + \left[1 - \left(\frac{v_c}{v_l}\right)^2\right]s_L\right\}P_L P_I \quad \ldots (37)$$

where n_w is the number of active wheels. The cut-off speed v_c may be different to that used for the tangential lofting analysis, because the aircraft and stone speeds are not necessarily equal. The number of partial stone encounters is therefore approximately an order of magnitude less than that for fully over-rolled stones, but previous studies have suggested that lofts at significant speeds tend to arise due to interactions at the sides of the tyre[4]. Since the above assumptions were based on preliminary lofting simulations with a cylindrical tyre, further investigation was required to gauge the accuracy of these assumptions under more realistic conditions. Therefore Section 3 describes the implementation of these enhanced lofting models.

3.0 PREDICTIVE MODELLING

A dynamic non-linear explicit finite element analysis program, LS-DYNA 971[15], was used to simulate a tyre rolling over a spherical stone at typical aircraft take-off speeds and loads (Fig. 5). Details of the surface of the tread, such as grooves, were not included in the finite element mesh, because interactions with the groove were considered to be a special case and the groove depth would depend on the degree of wear of the tyre. The wheel rolled over the stone whilst maintaining a predetermined offset distance from the stone's centre. The density of the rim was adjusted to model the aircraft weight and give the wheel a high enough inertia to prevent the stone influencing the wheel's motion. This removed the need for additional constraints on the wheel along the direction of the axle. Damping was applied to reduce any vibrations around the circumference of the tread which could influence the contact velocity with

https://doi.org/10.1017/S000192400000333X Published online by Cambridge University Press

Table 1
Parameters used to define the boundary conditions in the LS-DYNA model

Parameter	Value
Stone diameter	20mm
Proximity	30%
Aircraft speed	70ms^{-1}
Tyre outer radius	0·37m
Tyre-stone friction (static, kinetic)	0·65, 0·6
Ground friction (static, kinetic)	0·6, 0·5

the stone. These vibrations were artefacts of the finite element model and were introduced when the tyre was inflated. The case of stone crushing was not of primary interest but the principal stresses for stone fracture or shattering were checked. The nominal parameters in the simulation are shown in Table 1 and the material properties, which assumed quasi-static conditions, are shown in Table 2. The material properties for the aircraft tyre material were based on a series of tension and compression tests to measure the constitutive relations of samples cut from an aircraft tyre tread[16].

3.2 Development of inflated rolling tyre model

The original cylindrical solid tyre model described in Ref. 2 was further developed by initially using quadrilateral and triangular Belytschko-Tsay shell elements to form an aircraft tyre mesh (Fig. 5). The shell elements used an orthotropic elastic material model with the nine orthotropic constants[18] derived using the theory of composites[19]. Eight-node solid elements were later used to provide an enhanced representation of the through-thickness response of the rubber, along with the Mooney-Rivlin material model[20]. These solid elements were generated by extruding the original surface mesh, so that the shell and solid elements were connected by merged nodes. The tyre had a tread thickness of 30mm, was inflated to 1·5MPa and was travelling at a speed of 70ms^{-1}, which is the maximum take-off speed used for a C-130 Hercules operating at its maximum take-off weight. The coefficients of static and kinetic friction were 0·65 and 0·6 for the tyre-stone interface and 0·6 and 0·5 for the stone-ground interface respectively. The inflated tyre model containing both shell and solid elements gave similar values for the total speed of the stone to that obtained using only shell elements, 3·16ms^{-1} and 2·97ms^{-1} respectively, but the vertical velocity component decreased from 2·17ms^{-1} to 1·18ms^{-1}. The deflection was governed by the membrane stresses in the shell elements rather than the local indentation of the tread rubber. This was verified by repeating the analysis using shell elements having only membrane stiffness and noting that the loft velocity (the speed at which the stone was projected from the tyre) changed by only 8·2%.

3.2.1 Validation of inflated tyre model

A simulation was formulated to validate the inflated tyre model (Fig. 6) against the experimentally measured load-indentation relationship of a tyre from an Aztec aircraft. In this simulation, a rigid body

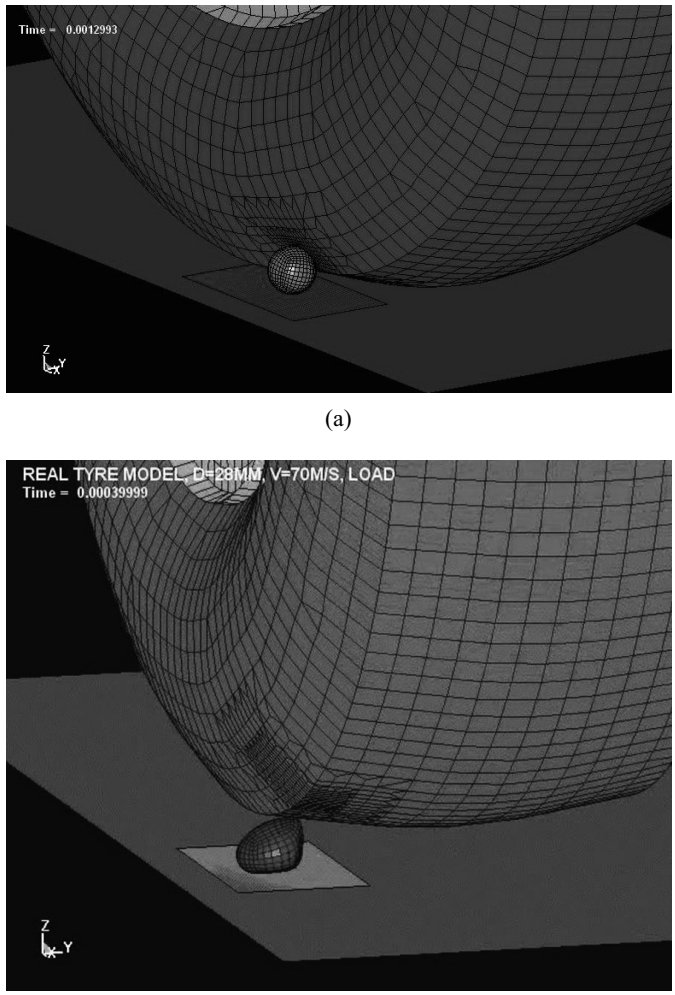


Figure 5. FE model of a C-130 nose tyre inflated to 1·5MPa partially rolling over (a) a 28mm spherical stone and (b) a smooth irregular stone with a maximum dimension of 34mm, just prior to lofting.

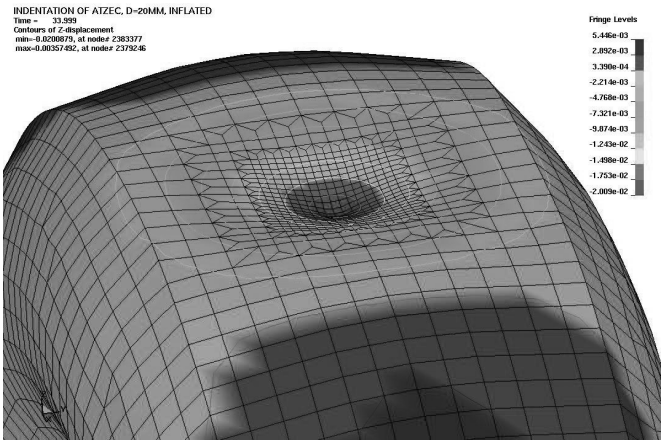
constraint was applied to the tyre hub to model the support structure, which in the experiment consisted of a steel frame and steel shaft[16] (Fig. 7). Quasistatic conditions were simulated by using mass scaling with a time step scale factor of 0·01. This enabled the simulation indentation speed to be set to the same speed as the test speed of 50mm/min. The 20mm diameter indenter head was modelled using the geometric spherical rigid wall option in LS-DYNA with a prescribed displacement of 24mm. In the experiment, digital image correlation (DIC) was used to measure the 3D displacement and strain fields in the vicinity of the indenter. The DIC instrumentation used for acquiring strain measurements was the Aramis system

Table 2
Properties of the material definitions used in the LS-DYNA models (Source: CES Software[17])

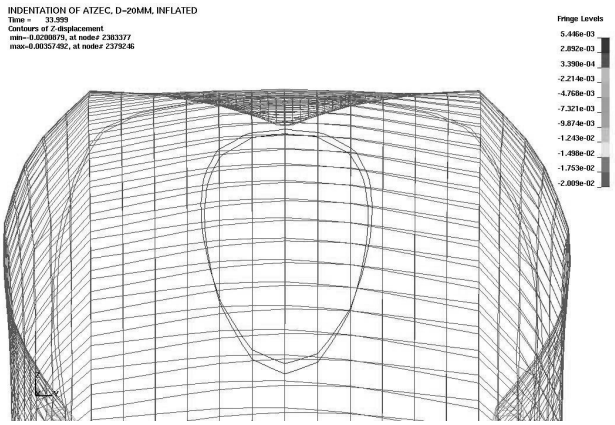
Material	Young's Modulus, E (GPa)	Density, ρ (kg/m^3)	Poisson's ratio, ν
Concrete	Rigid [25]*	2,350	0·15
Stone	Rigid [50]*	2,700	0·25
Aluminium	Rigid [70]*	2,700	0·33
Tyre rubber	Experimental stress-strain curve[16]	1,000	0·495

**Values in square brackets are values used by LS-DYNA in contact calculations.*

https://doi.org/10.1017/S000192400000333X Published online by Cambridge University Press



(a)



(b)

Figure 6. (a) Isometric and (b) front views showing surface displacement field contours of the simulated tyre under indentation by a 20mm diameter tup at a maximum displacement of 24mm.

supplied by GOM using software version 5.3.0[21]. Two 1·3 megapixel cameras were mounted with an intersection angle of 25° such that both cameras viewed the indentation zone lit by two strip lamps. The cameras were connected to a computer-controlled trigger box which captured one image every second. The tyres were first sprayed black with a white speckle pattern to achieve a high contrast. The tyre inflation pressure was adjusted and measured using a standard car tyre foot pump with a pressure dial gauge.

The simulation predicted an almost linear relationship over the range of indentation displacements applied and the predicted compliance was slightly less than the measured indentation compliance (Fig. 8). At maximum displacement, the predicted and measured loads coincided, but greater hysteresis was found under experimental conditions. By integrating the unloading portion of the curve, an estimate of the maximum potential energy that could be released from the tyre during lofting was estimated. The maximum predicted and measured energies were 21·1J and 19·9J respectively, giving a 6% difference, with the prediction being conservative. At the point of transition between loading and unloading when the indenter head changed direction, the numerical simulation displayed a sudden decrease in load due to dynamic effects. This discontinuity was not seen in the experiment where the deceleration of the indenter was limited by the testing machine inertia.

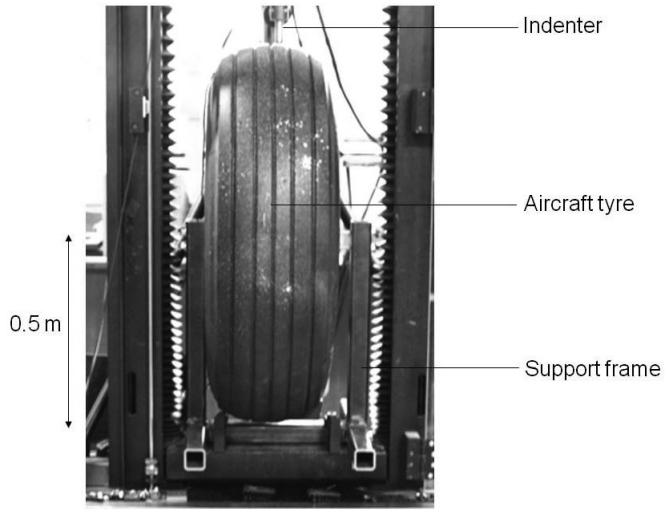


Figure 7. Experimental set up of indentation test on an aircraft tyre using a 20mm diameter hemispherical indenter.

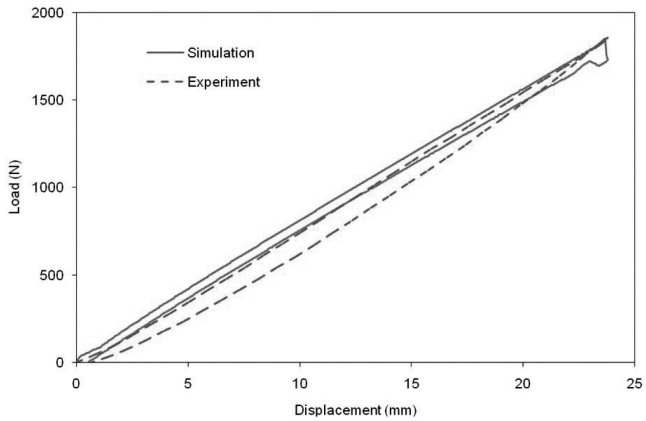


Figure 8. Load indentation behaviour of an Aztec tyre inflated to 0·34MPa showing the numerical simulation and experimental results.

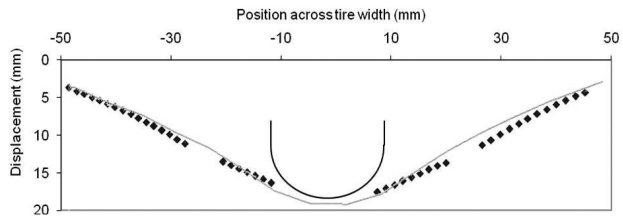


Figure 9. Displacement across the width of an Aztec tyre inflated to 0·34MPa at maximum indentation.

The displacement profiles were also compared at cross-sections across the tyre width (Fig. 9) and along the tyre circumference (Fig. 10). Note that the points not included in the experimental curve correspond to the grooves in the tread and the area under the indenter head. These areas were not visible to the DIC camera system used to measure the displacement field. The simulated profile across the width demonstrated greater changes in curvature around the indenter head than in the experiments. In the experimental profile, there was a small convex curvature across each portion of tread that was separated by the grooves. As expected, the simulation was unable to account for the local changes in curvature caused by the presence of the grooves.

https://doi.org/10.1017/S000192400000333X Published online by Cambridge University Press

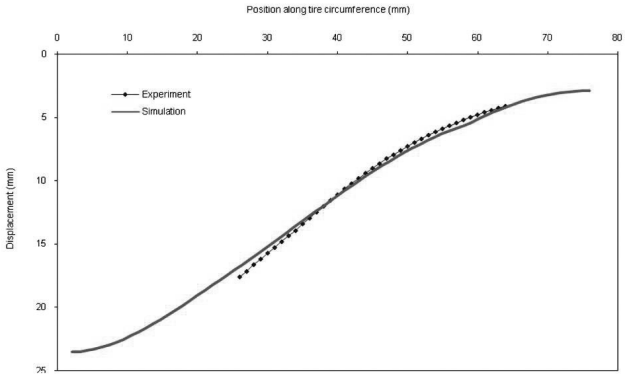


Figure 10. Displacement along the circumference of an Aztec tyre inflated to 0·34MPa at maximum indentation.

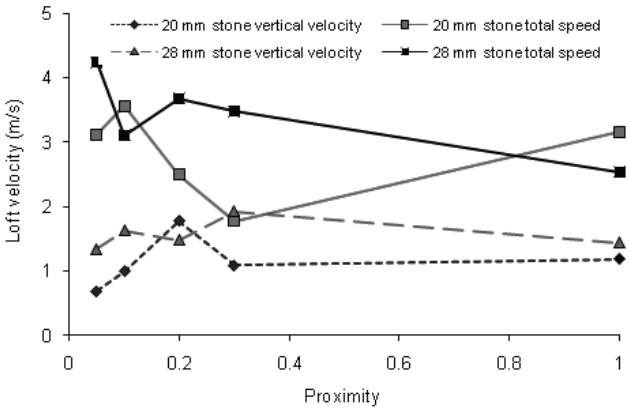


Figure 11. Loft velocities of 20mm and 28mm diameter spheres over-rolled by an inflated tyre at various lateral positions between the edge and the centreline of the tyre.

The tyre displacement profile along the circumferential direction is shown in Fig. 10. Again the points close to the indenter head could not be measured experimentally and only one side was visible. The predicted and measured displacement fields in the circumferential direction were in better agreement for most of the measured range. However the curves began to deviate closer to the indenter head, with the experimental displacement dropping below the predicted values.

3.2.2 *Lofting simulation*

The lofting of spherical stones of diameters 20mm and 28mm, using the material properties defined in Table 2, were simulated with each stone placed at five different locations across the width of the tyre with an aircraft speed of 70ms^{-1} (Fig. 11). The stone sizes were chosen to give masses corresponding to maximum expected runway debris impacts energies[22,23] of 19J and 50J at the average take-off velocity for a Hercules[1]. These positions, which in previous models were specified in terms of percentage overlap[2], were more conveniently denoted in terms of a non-dimensional parameter called the proximity. The proximity was the distance between the outer sidewall of the tyre and the centre of the stone divided by the half the width of the tyre. Therefore a proximity value of zero meant that the centre of the stone was aligned with the edge of the tyre and a proximity of unity meant that the centre of the tyre coincided with the centre of the stone. The simulated data points were concentrated towards the shoulder of the tyre, where a greater variation in the loft velocities was expected. For most values of proximity, the larger stone was lofted at higher speeds, and the variation in loft velocities for the larger stone was smaller.

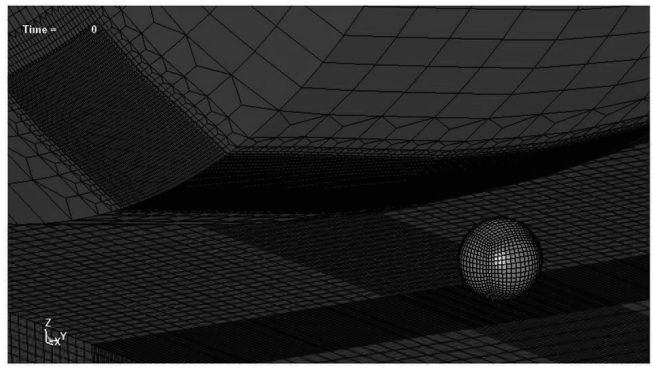


Figure 12. Initial FE simulation geometry for a 20mm diameter stone over-rolled by a tyre inflated to 0·34MPa.

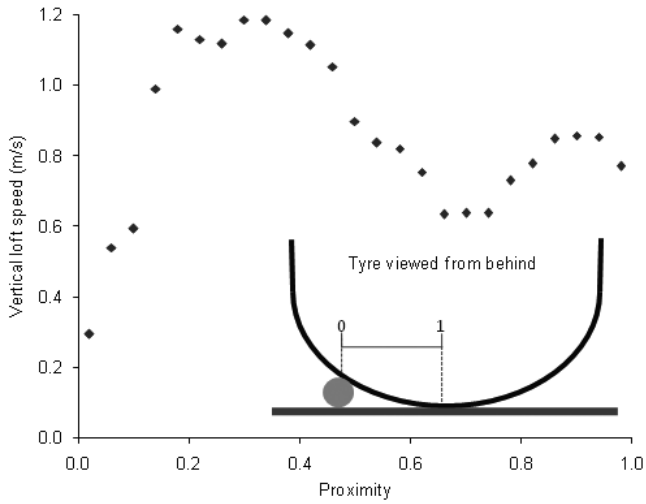


Figure 13. Numerical simulation results showing the vertical loft speed of a 20mm diameter stone as a function of position relative to an over-rolling tyre of outer diameter 0·74m at a speed of 70ms^{-1}.

Compared to simulations using a cylindrical solid tyre[2], where the stone loft velocities were up to 30ms^{-1}, the inflated tyre model predicted much lower speeds; not exceeding 5ms^{-1}. The suppression of lofting in these simulations was attributed to the shallow angle at which the surface of the tyre rubber made contact with the stone. For the inflated tyre, the curvature near the tyre shoulder meant that the maximum possible contact angle above the horizontal was approximately 30° for the largest realistic stones found on runways. This hypothesis was checked by returning to the solid tyre model and observing that for contact angles less than 75° above the horizontal, lofting was prevented as the stone could not escape sideways. Further evidence of this phenomenon was provided by experimental impacts with a chamfered impactor head[2].

The results for the 20mm stone were explored in greater detail using a tyre with a fine mesh across the full spectrum of proximities tested (Fig. 12). A space-filling Monte Carlo analysis in LS-OPT 3.2 was used to obtain plots of the vertical loft velocity for 25 different stone positions. Independently, both the stone and ground were modelled as elastic materials to check the influence of the compliance of each on the loft speeds but the lack of significant changes in the results demonstrated that the simulations were not sensitive to these parameters.

The vertical loft speeds as a function of the position of a 20mm diameter stone relative to the tyre are presented in Fig. 13. All of the prescribed speeds were under 1·2ms^{-1}. A range of proximity values of between 10% and 45% led to velocities exceeding 1ms^{-1}, but for

https://doi.org/10.1017/S000192400000333X Published online by Cambridge University Press

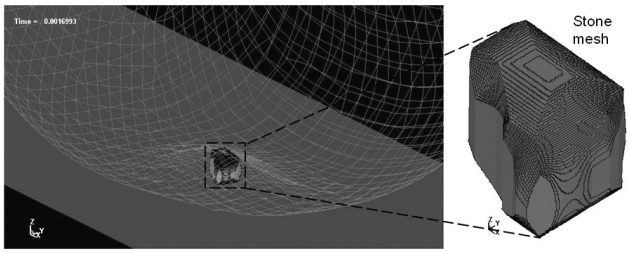


Figure 14. Finite element model of an inflated tyre rolling over a 31mm rough irregular stone.

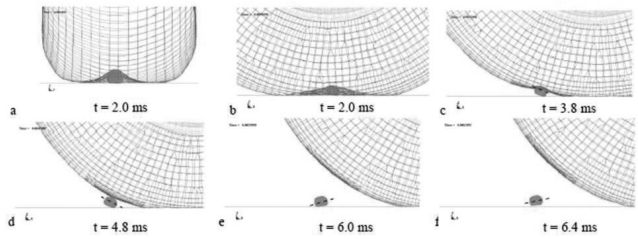


Figure 15. (a) Front view of a tyre rolling over a 31mm rough irregular stone and (b)-(f) side view sequence of images of the tyre rolling over a 31mm rough irregular stone at 70ms^{-1}. A dashed line is used to illustrate the rotation of the stone.

stone positions with a proximity of less than 10%, the vertical loft speed quickly approached zero, whilst proximity values greater than 45% led to a more gradual decrease in loft speed. A small increase in loft speed was observed for stones very close to the central plane of the tyre, where the stone experienced a nearly symmetric loading.

3.3 Irregular stone models

A smooth irregular stone mesh (Fig. 5(b)) was generated by creating a separate LS-DYNA model consisting of six rigid walls surrounding a solid sphere of plastic material with a low stiffness. The sphere was given an initial velocity such that it rebounded off multiple walls in arbitrary directions to deform the sphere. This produced a stone with a combination of flat and curved surfaces, providing a shape with geometric parameters (aspect ratio and circularity) matching the average values for stones collected and analysed from UK RAF runways[1]. The resultant nodal geometry obtained from this smooth stone generation model was used as the input mesh for the rolling tyre model after changing the material characteristics to match those of real stones. This process enabled complex and realistic stone shapes to be generated very quickly, but was limited to smooth surfaces only. Under the same nominal conditions as the previously described simulations for the spherical stones, this stone was lofted at an absolute speed of 4·56ms^{-1} and a vertical velocity of 1·65ms^{-1}.

The mesh for a rough irregular stone (Fig. 14) was constructed directly from a photograph of a stone collected from a runway at RAF Lyneham, UK[1]. The photograph was imported into image processing software (Image J) and converted into a binary image to allow the outline to be saved as *x-y* data. By reading the *x-y* data points into LS-PREPOST and extruding the profile, a solid prismatic mesh was generated. The sharp cornered surfaces of this prism were cut away at angles to remove the flat top and bottom surfaces and gave the stone a more realistic profile and mass. The generation of the 3D geometry was based on the assumption that the geometrical characteristics of the stone from a side view were equivalent to those from a plan view. Solid elements were chosen so that the mass and inertia properties could be calculated correctly.

During these simulations, the low contact angles meant that the difference between partial and complete over-rolling scenarios was trivial and the proximity of the stone only determined the degree to which the tread was indented. In both cases, the downward force applied by the tyre shifted from the back to the front surface of the stone and its magnitude reached a maximum when the tyre axle passed directly over the centre of the stone, coinciding with the greatest tread deformation. However, most of the stored strain energy was recovered by the tyre so that at the instant the stone was released from the tread, the force on the stone had reduced significantly and the stone was pushed back towards the ground at a low speed and bounced upwards with a speed of 4·97ms^{-1} and vertical velocity of 4·63ms^{-1}. In the absence of aerodynamic effects, this corresponded to a maximum height of 1·09m.

For a spherical stone, when the surface of the tread was released from the stone, it did not result in significant motion of the stone. For an irregular stone, the trailing surface of the stone was dragged forward by the back of the tread surface, leading to an initial forward tumbling of the stone (Fig. 15). The stone retained a slight forward velocity component due to the tread travelling forwards as it was raised from the ground, but since this was small in comparison to the aircraft speed, it had little influence on the probability of impact.

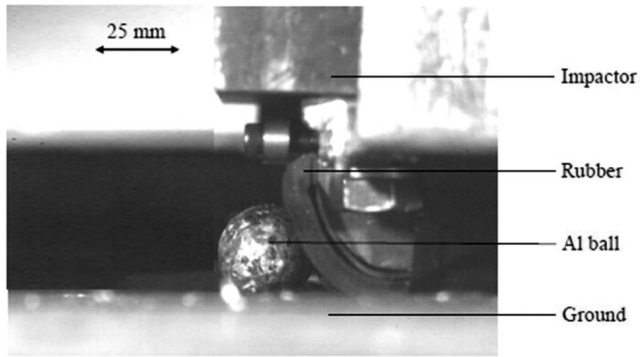


Figure 16. High speed video image of a drop weight impactor covered with 7·5mm thick reinforced rubber striking a 25mm diameter aluminium ball.

4.0 DROP WEIGHT IMPACT EXPERIMENTS

Comparisons between FE models of a wheel dropping vertically onto a stone and a wheel rolling over a stone suggested that using a drop weight impact might be a valid approach for conducting simple preliminary lofting experiments under controlled conditions. To validate the numerical simulations, tests were conducted using a modified 65kg drop weight impactor capable of reaching kinetic energies of over 2kJ[2]. In the experimental studies, aluminium balls were used to represent spherical stones, and reinforced rubber was attached to the bottom surface of a steel impactor to simulate a tyre tread. The base was a steel block mounted on four springs to reduce damage to the impactor. In previous experiments[2], various grades of sandpaper were attached to the base surface to mimic a realistic surface roughness.

An improvement in the repeatability of the experiments was made by using a machined surface with an intersecting pattern of fine grooves to give a roughness similar to that of a runway surface. Further refinements included introducing a lubricated mechanical guide to provide a more consistent alignment of the falling impactor and extending the tests to greater drop heights of up to 3m to determine the effect of the impact speed. A Phantom V7 high speed camera at a resolution of 800 × 600 pixels, a frame rate of 4,000f/s and an exposure time of 48μs was used to record the lofting events (Figs 16 and 17). The Phantom 640 image analysis software was used to deduce the speed and loft angle of the balls as well as the impactor drop speed. In addition, a small number of tests were also carried out on real stones and aluminium nuts to ascertain whether the lofting mechanisms were similar to those obtained for spheres.

https://doi.org/10.1017/S000192400000333X Published online by Cambridge University Press

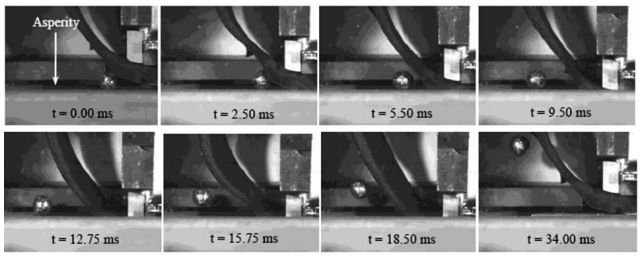


Figure 17. Asperity lofting of a 25mm Al ball initially launched sideways by a descending Hercules tyre section.

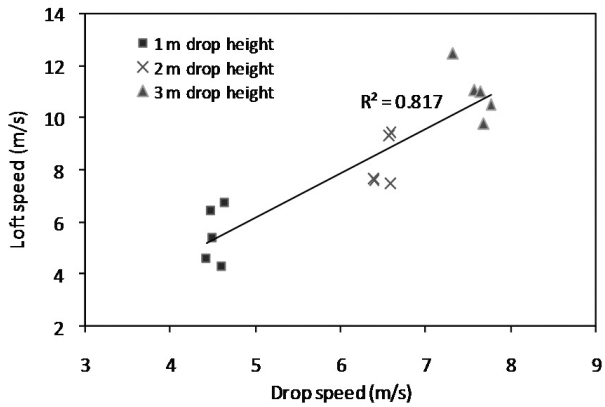


Figure 18. Loft velocity against impactor speed for a 25mm diameter ball struck by a section from a Hercules tyre.

4.1 Effect of rubber thickness

Tests were performed using various thicknesses of rubber attached to an impactor head with an edge radius of 25mm as shown in Fig. 16. The rubber thicknesses were 6mm, 7·5mm, 9mm, 10·5mm and 12mm. The 25mm diameter ball was found to be lofted to angles of up to 30° for rubber thicknesses of 6mm and 7·5mm but lofting was suppressed when the thickness of the rubber was equal to or greater than 9mm, in which case either no motion or purely horizontal motion of the ball was observed. With a rigid curved impactor covered by a thin sheet of rubber, the rubber was not able to deform or indent sufficiently to envelop the stone. Thus, for the thin rubber material, the mechanism was best described by the hammer model (Fig. 2(b)). For thicker rubber layers, the pinch mechanism (Fig. 2(c)) was appropriate, whereby the motion of the stone was essentially horizontal, which could not directly explain the impact damage that has been observed on structural parts of aircraft such as the C-130 Hercules (Fig. 1). However, the launch speeds observed were large enough that vertical velocity components produced by subsequent asperity lofting (Fig. 2(d)) could result in impacts with aircraft structures.

4.2 Tests using a tyre section from a C-130 Hercules aircraft

In tests using a C-130 Hercules aircraft tyre attached to the impactor (Fig. 17) there was no evidence to suggest that the stones could stick to the tyre tread when they are enveloped, either when there was partial or complete overlap between the tyre and the stone. Instead, when the stone was a within a narrow range of positions close to the shoulder of the tyre, loft angles of less than 5° above ground could occur, but for the majority of instances the stone would not escape, as witnessed in the numerical simulations. The 25mm aluminium

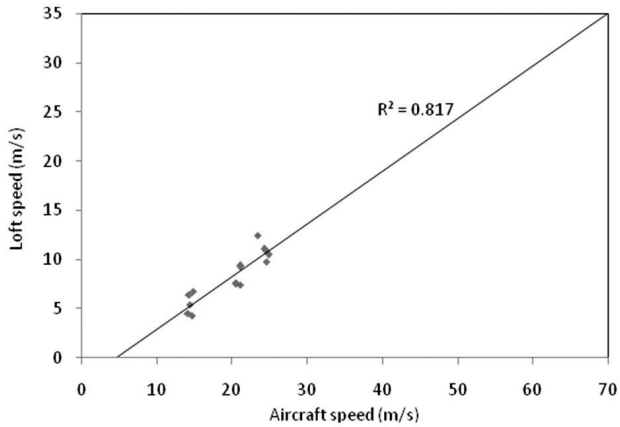


Figure 19. Loft velocity against aircraft speed for a 25mm diameter ball.

ball travelled with a backspin angular velocity of approximately 1,300rad/s, such that the rotational kinetic energy contributed to 68% of its total kinetic energy of 6·7J. Asperity lofting could occur if an irregular stone was made to spin and at the same time launched horizontally along the ground. Any bumps on the surface of the spinning stone may hit the ground and give the stone an upward velocity component. Alternatively, the stone launched horizontally may strike a protrusion (asperity) from the ground (Fig. 17). Based on these experiments, the stone launch speeds for higher drop speeds could be conservatively predicted by assuming a linear relationship between the stone loft speed and the impactor drop speed (Fig. 18). The relationship in Equation (1) of Ref. 2 between the vertical velocity component of the descending tyre section and the aircraft speed was then used to relate the loft speed to the aircraft speed (Fig. 19). A major assumption required for this extrapolation was that rate effects did not become important at higher speeds. The effect of this assumption is discussed in Section 5.

5.0 DISCUSSION

5.1 Lofting simulation

A comparison between the simulated and measured indentation responses of an aircraft tyre showed that both the predicted compliance and hysteresis were underestimated leading to an overestimation of the potential energy that could be released from the deformed tyre. These differences, coupled with the discontinuity in the displacement cross-section across the width but not along the circumference suggested that the presence of the tread grooves was the main shortcoming of the implemented inflated tyre model. Using an experimental load-indentation curve for an Aztec aircraft tyre, the maximum energy that the tyre could transmit to a stone based on a conservative linear fit to the quasi-static load-indentation relationship was 20J[16]. A typical 20mm diameter spherical stone with a density of 2,680 kg/m^3 could therefore achieve a maximum velocity of 52ms^{-1} if all the potential energy was converted to translational velocity. However the simulations predicted speeds no greater than 5ms^{-1}. Most of the energy was simply returned to the tread and dissipated by other processes including hysteresis and noise. A 5ms^{-1} loft speed would enable the stone to reach a height such that leading edges of aircraft under-structures could impinge on the stone. However, the time required to reach that height meant that the aircraft to must have travelled sufficiently slowly to avoid simply passing overhead. From the geometry of the C-130 Hercules given in Fig. 3, this maximum impact speed was estimated to be approximately 30ms^{-1}.

https://doi.org/10.1017/S000192400000333X Published online by Cambridge University Press

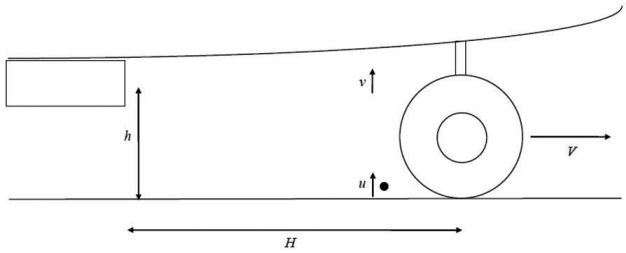


Figure 20. Schematic of geometry and velocities used to calculate minimum loft velocity required for impact.

The lofting simulations demonstrated that using a more realistic shaped tyre reduced the effect of the stone position compared to the influence of overlap for a sharp edged tyre. Instead, the roughness or irregularity of the stone surface was considered important for the tyre to build up lofting forces. Spherical or smooth irregular stones followed a rocking motion along the ground, where the top surface was dragged along by the tyre tread. The relative motion between stone and ground meant that the tread was able to regain its shape in a steady fashion upon passing the stone so that a steady unloading occurred with no significant lofting. Rough irregular stones that were unable to rotate when passed over by a tyre led to a more abrupt change in the tyre unloading.

Although the simulation findings made it difficult to explain the damage occurring to aircraft such as the C-130 Hercules, the low loft speeds predicted by the improved simulations were in agreement with an independent set of experiments carried out using a tyre driven over a circular track containing stones[4]. In that study it was reported that "the only mechanisms observed with substantial vertical velocity components involved stones being launched laterally from the edges of tyre treads… Launch velocities were mainly less than 2·5ms^{-1}. The probability of launching debris to above 4ms^{-1} was about 0·03. Angularity and size both increase lofting probability." All of these findings were consistent with the results of the present simulations. However, the 3% of cases for which launches occurred above 4ms^{-1} were best explained by mechanisms not included in the current models such as groove lofting[3], and asperity lofting.

5.2 Minimum loft velocity for impact

Given the modest loft velocities observed, the primary source of damage hinges upon whether the stone is able to reach heights such that any leading edge structures could intercept its path. Assuming negligible air resistance, the constant acceleration equations were used to estimate the minimum loft velocity for a stone to impinge on part of the aircraft. The vertical velocity of the stone upon impact v was expressed in terms of the initial vertical loft velocity u, the time t required for the aircraft to travel a distance H and the height h at which the impact occurs (Fig. 20),

$$v = u - \frac{1}{2}gt \quad \ldots (38)$$

$$v^2 = u^2 - 2gh \quad \ldots (39)$$

Substituting Equation (38) into Equation (39) leads to

$$u^2 - ugt + \frac{1}{4}(gt)^2 = u^2 - 2gh \quad \ldots (40)$$

$$u = \frac{2h}{t} + \frac{gt}{4} \quad \ldots (41)$$

Assuming the aircraft maintains a constant speed, such that $t = H/V$,

$$u = \frac{2hV}{H} + \frac{gH}{4V} \quad \ldots (42)$$

For h = 0·6m, V = 55ms^{-1}, H = 10m, the initial vertical loft velocity was u = 7·0ms^{-1}. In other words, for an aircraft travelling at 55ms^{-1}, the stone must be lofted at a speed greater than 7ms^{-1} upwards to strike a structure 0·6m above the ground before it passes overhead. This assumes the stone has no velocity component along the aircraft's path and air resistance is not taken into account.

To explain the damage to the undersurface of the Hercules aircraft, other conditions that were not accounted for in the present simulations include aerodynamic effects. Even in the experiments by Bless *et al*[4], the aerodynamic effects were not fully accounted for because only a tyre was used rather than a complete aircraft structure. The Magnus effect[24-26] could produce lift on a stone made to rotate with backspin relative to the airflow beneath the undercarriage. Despite the low translational speed of the lofted stones, provided there is a significant flow velocity in the wake of the landing gear, a stone may be able to achieve a net upward acceleration. However the wake behind a rolling wheel is highly turbulent[27], and hence a spinning stone would be highly unlikely to achieve a significant net lift, despite the presence of high velocities within the vortices. A steady laminar wake owing to the air dragged forward by the underbelly of the aircraft was considered to have a greater influence on the stone's path. The drag and lift forces acting on a stone with radius r, angular velocity ω and spin ratio S can be calculated using the following equations[25]

$$F_D = \frac{1}{2}C_D \rho v^2 \pi r^2 \quad \text{and} \quad F_L = \frac{1}{2}C_L \rho v^2 \pi r^2 \quad \ldots (43)$$

$$\text{where } C_L = f(S, \mathrm{Re}) \; S = \frac{r\omega}{v} \quad \text{and} \quad \mathrm{Re} = \frac{2\rho v r}{\mu} \quad \ldots (44)$$

These aerodynamic effects are expected to have greater influence on smaller stones due to their higher spin rates and lower terminal velocities. Even for the smallest stones that are able to cause significant damage upon impact, the resulting vertical velocity component would not directly damage horizontally-oriented structures, such as the fuselage. However, aerodynamic effects may contribute to the heights predicted in the current lofting simulations, such that the combined effects are sufficient to cause leading edge impacts or glancing impacts when the aircraft is in the rotation phase of take-off. Considerable further investigation into the interaction between the airflow around an aircraft undercarriage and lofted runway debris would be required to confirm whether or not a purely solid mechanics approach to the problem is valid.

5.3 Drop weight impact experiments

The drop weight experiments had limitations in reproducing the conditions encountered by stones whereby a gradual loading-unloading cycle of vertical forces and horizontal tractions would be applied. Additionally, near the contact zone between the stone and the tyre, the support conditions within the tyre did not fully correspond to the structure behaviour of an inflated tyre. Due to the nature of the attachment to the impactor, the section of tyre directly beneath the impactor head was stiffer than the actual scenario, whereas to the side of the impactor head, the tread had greater compliance. Nevertheless, it was clear that the geometry of the Hercules tyre did not allow the stone to be flicked upwards in a similar way to previous experiments using reinforced rubber sheet[2]. In the present experiments, at almost all levels of proximity, the stone was simply pushed into the ground and had a small remnant rebound speed after the impactor ascended, in agreement with the simulations. For irregular stones, the same pattern of events was expected, regardless of the stone position. For the spherical stones at positions very close to the tyre edge, the purely sideward back-spinning launches

https://doi.org/10.1017/S000192400000333X Published online by Cambridge University Press

observed in the experiments but not in the simulations were attributed to some degree of shearing failure at the lower surface of the stone. Evidence of this shearing was provided by the emission of small fragments just as the stone began to spin. Hence, a further development of the model could be to introduce elements close to the contact zone between the ground and the stone. These elements, which may be attached to either the stone or ground, would fail at the appropriate shear stress level. However, the predominantly horizontal motion of the stone would still require another mechanism to generate significant vertical velocities.

Given the high speeds at which stone lofting events take place, the strain rate sensitivity of the tyre material may also play an important role in the determining the loft speeds obtained. Experiments on rubber at high strain rates report a small stiffening effect in both tension and compression[28] due to a relaxation time associated with the movement of long chain molecules in the rubber material[29]. Accurately quantifying the influence of the rate-dependent stiffening on the tyre response is complicated by the varying strain rate during the over-rolling event, whereas typical constitutive data is measured at constant strain rates. Qualitatively, the quasi-static material properties used in the simulations would therefore have over-predicted the tyre compliance and under-predicted the peak force applied to the stone. Additionally, the tyre structure would approach the conditions prescribed in the drop weight experiments, where the tread was supported by a solid impactor head rather than by pressurised air. As a consequence, the actual lofting mechanism would tend towards hammer lofting as opposed to pinch launching, reinforcing the validity of predicting the loft velocities at high aircraft velocities using a hammer model.

6.0 CONCLUSIONS

This investigation aimed to realistically model the lofting of runway stones by tires to predict the likely impact threat to aircraft. A finite element model of a tyre rolling over a stone was developed to predict vertical loft speeds of stones under typical take-off conditions. Comparison of quasi-static indentation of the aircraft tyre in the simulation and in the experiment demonstrated a difference of 6% in the potential energy that could be transferred to an over-rolled stone. The simulations predicted vertical speeds no greater $5ms^{-1}$ for all types of stones including spherical, smooth irregular and rough irregular stones, with the latter exhibiting the highest speeds. The implication was that only leading edge strikes were considered as viable causes of damage, and horizontally-oriented structures could only receive highly oblique impacts during the rotation phase of take-off and at touchdown. Consequently, the assumption that the impact velocity was equivalent to the instantaneous aircraft speed, and hence the probabilistic equations described in Section II were concluded to be appropriate for predicting the probabilities of stones exceeding critical impact energies.

Experiments using a drop weight impactor were used to validate the mechanisms observed in the rolling tyre models. Aluminium balls struck by a steel impactor covered with reinforced rubber were seen to exhibit hammer lofting for rubber layers of 7·5mm thickness or less. Thicker rubber layers, as more common in aircraft tires, resulted in either no significant stone movement or pinch launching within a narrow range of stone positions near the edge of the impactor, which could be followed by asperity lofting for rough runways or highly irregular stone shapes. Further work to investigate this mechanism would involve characterising the roughness of commonly used runways in terms of the sizes and frequencies of the surface asperities. The importance of the contact angle and tread thickness was confirmed by attaching part of an aircraft tyre to the impactor head for a better representation of the material and geometric properties of the tyre. The low angle but significant velocity launches of stones observed in the experiments but not in the simulations were attributed to the high stiffness of the test rig impactor head, which represented an unrealistically high inflation pressure. An improved correlation with the simulations is expected from a more sophisticated full-scale set-up involving an inflated tyre driven over a debris strewn runway. Predictions obtained from the experimental results, which were extended to realistic aircraft take-off speeds, concluded that absolute loft speeds would not exceed half the aircraft speed.

The current study has concluded that lofting to high vertical speeds is a rare event and that the irregularity of stones plays some role in increasing the probability of lofting. Hence a suggested route for future studies would be to develop a method to automatically generate numerical models of realistic rough irregular stones and automate the process of running the lofting simulations continuously. A sequence of Monte Carlo simulations would then be set up with the number of runs of the order of the expected number of stone encounters in an aircraft's lifetime. An additional refinement would be to couple the simulations with the fluid-structure interaction capabilities of LS-DYNA to include post-lofting aerodynamic effects. Finally, further work to simulate the realistic impact of debris on aircraft structures will also be investigated experimentally by projecting stones onto aircraft composite materials at speeds representative of take-off conditions using a medium velocity impactor, such as the crossbow impactor developed at Imperial College London. The improved understanding of the underlying physics of the stone lofting and impact damage mechanisms gained through these studies can be used to identify the critical conditions that result in severe damage from runway debris, and underpin a probabilistic approach for damage tolerant design or certification.

ACKNOWLEDGMENTS

The authors would like to acknowledge the support of UK MoD, particularly Nick Deavinn and technicians at RAF Lyneham for providing valuable information relating to impact damage occurring to the C-130 Hercules. Appreciation is also expressed to EPSRC and Dstl for funding this research, Sally Longstaff for her contribution to the experimental drop weight studies and Michael Graham for support regarding the aerodynamics of debris lofting.

REFERENCES

1. GREENHALGH, E.S. Characterisation of the realistic impact threat from runway debris, *Aeronaut J*, 2001, **105**, (1052), pp 557-570.
2. NGUYEN, S.N., GREENHALGH, E.S., OLSSON, R., IANNUCCI, L. and CURTIS, P.T. Modeling the lofting of runway debris by aircraft tires, *J Aircr*, 2008, **45**, (5), pp 1701-1714.
3. NGUYEN, S.N., GREENHALGH, E.S., OLSSON, R., IANNUCCI, L. and CURTIS, P.T. Parametric analysis of runway stone lofting mechanisms, 2009, submitted for publication.
4. BLESS, S.J., CROSS, L., PIEKUTOWSKI, A.J. and SWIFT, H.F. FOD (foreign object damage) generation by aircraft tires, 1983, Dayton University, OH, Research Inst, Defense Technical Information Center, Rept. A913331.
5. BOWEN, R., BLEAY, S., GREENHALGH, E.S., LORD, S., MEW, A. and WILLOWS, M. Certification of composite structures with impact damage: a review (UC), 1998, CR980550/1.0, Defence Evaluation and Research Agency, Material Science Section, UK.
6. HADEKEL, R. The mechanical characteristics of pneumatic tyres, 1952, S & T memo 10/52, Ministry of Supply, London, UK.
7. OLSSON, R., DONADON, M.V. and FALZON, B.G. Delamination threshold load for dynamic impact on plates, *Int J of Solids and Structures*, 2006, **43**, (10), pp 3124-3141.
8. OLSSON, R. Experimental validation of delamination criterion for small mass impact, 2007, Paper GE223247, Vol 1, Kyoto, Japan.
9. BEATTY, D.N., READDY, F., GEARHART, J.J. and DUCHATELLIER, R. The study of foreign object damage caused by aircraft operations on unconventional and bomb-damaged airfield surfaces, 1981, Report No. ADA117587, BDM Corp Mclean, VA, USA.
10. TAYLOR, M.J.H. *Flight International World Aircraft & Systems Directory*, 2002, Reed Business Information, Surrey, UK.

https://doi.org/10.1017/S000192400000333X Published online by Cambridge University Press

11. JACKSON, P. *Jane's All the World's Aircraft 2007-2008*, 2007, Jane's Publishing, London, UK.
12. ZAMMIT-MANGION, D. Simplified algorithm to model aircraft acceleration during takeoff, *J Aircr*, 2008, **45**, (4), pp 1090-1097.
13. CHENG, A. Discussion of approaches to estimate the aircraft stopping distances under standard operating procedures, 2007, NTIS, DOT/FAA/AR-TN07/21, USA.
14. KIM, B.J., TRANI, A.A., GU, X. AND ZHONG, C. Computer simulation model for airplane landing-performance prediction, *Transportation Research Record*, 1996, (1562), pp 53-62.
15. HALLQUIST, J.O. LS-Dyna Theoretical Manual, Version 970, 1998, Livermore Software Technology Corporation, Livermore, California.
16. LONGSTAFF, S. Experimental characterisation of the interaction between tyres and stones, MEng final year project report, 2008, Department of Aeronautics, Imperial College London, UK.
17. ASHBY, M. and CEBON, D. Cambridge Engineering Selector, 2008, Computer Software, Granta Design, www.grantadesign.com.
18. CUITINO, A.M., SERNAS, V. and MCALLEN, J. Numerical investigation of the deformation characteristics and heat generation in pneumatic aircraft tires. 1. Mechanical modeling, *Finite Elements in Analysis and Design*, 1996, **23**, (2-4), pp 241-263.
19. JONES, R. *Mechanics of Composite Materials*, 1975, Hemisphere, NY.
20. MINES, R.A.W. and KARAGIOZOVA, D. Impact of aircraft rubber tyre fragments on aluminium alloy plates: II - Numerical simulation using LS-DYNA, *Int J of Impact Engineering*, 2007, **34**, (4), pp 647-667.
21. *GOM Aramis User Manual*, 2004, GOM, Braunschweig, Germany.
22. HACHENBERG, D. The role of advanced numerical methods in the design and certification of future composite aircraft structures, 2002, Vienna, Austria.
23. OLSSON, R. DAMOCLES Task I – Deliverable: A survey of impact conditions relevant in aircraft composite structures, 1998, FFAP H-1353, FFA – The Aeronautical Research Institute of Sweden, Bromma.
24. WATTS, R.G. AND FERRER, R. The lateral force on a spinning sphere: Aerodynamics of a curveball, *American J of Physics*, 1987, **55**, pp 40-44.
25. NATHAN, A.M. The effect of spin on the flight of a baseball, *American J of Physics*, 2008, **76**, (2), pp 119-124.
26. CHAKRAVERTY, S., STIHARU, I. and BHAT, R.B. Influence of aerodynamic loads on flight trajectory of spinning spherical projectile, *AIAA J*, 2001, **39**, (1), pp 122-125.
27. MCMANUS, J. and ZHANG, X. A computational study of the flow around an isolated wheel in contact with the ground, *J Fluids Engineering*, 2006, **128**, (3), pp 520-530.
28. MINES, R.A.W., MCKOWN, S. and BIRCH, R.S. Impact of aircraft rubber tyre fragments on aluminium alloy plates: I – Experimental, *Int J of Impact Engineering*, 2007, **34**, (4), pp 627-646.
29. HOO FATT, M.S. and OUYANG, X. Three-dimensional constitutive equations for styrene butadiene rubber at high strain rates, *Mechanics of Materials*, 2008, **40**, (1-2), pp 1-16.

https://doi.org/10.1017/S000192400000333X Published online by Cambridge University Press